J. Cosmet. Sci., 72, 519–546 (September/October 2021)

Characterization of Bleached Hair: Vibrational Spectroscopy, Thermal Analysis, and Determination of Equivalent Damage Factor

TIMOTHY GILLECE, LARRY SENAK AND ROGER L. MCMULLEN
Ashland LLC, Bridgewater, New Jersey, USA (T.G., L.S., R.L.M)

Accepted for publication May 27, 2021.

Synopsis

In this study, we sought to determine a practical correlation between disulfide bond oxidation and the thermal response of chemically bleached hair fibers. Bleaching processes, and the alkaline environment under which they are applied, cause scission of native covalent cystine cross-links in virgin hair fibers to form cysteine-sulfenic, cysteine-sulfinic, and cysteine-sulfonic (cysteic) acids in the cuticle, cortex, and, to a lesser extent, in the medulla. To further our understanding of hair bleaching kinetics, results from Fourier transform infrared (FTIR) chemical imaging, FTIR-attenuated total reflectance (FTIR-ATR), and Raman spectroscopic measurements were correlated with results from high pressure differential scanning calorimetry (HPDSC), dry differential scanning calorimetry (DSC), dynamic vapor sorption (DVS), and modulated thermogravimetric analysis (MTGA). Spectroscopic results were used to calculate an equivalent damage factor (EDF), which was used to index bleaching damage to the cuticular and cortical compartments of the hair fiber. Spectrofluorescence and colorimetry measurements were performed on bleached whole fiber hair tresses. Fluorescence measurements provided a means to monitor changes in the tryptophan and kynurenine levels, and colorimetry measurements were conducted to quantify the overall color change ($\Delta \boldsymbol{E}$) of hair at various bleaching intervals. FTIR imaging showed that cysteic acid levels in the fibers increased with increasing bleaching time and that the spatial distribution of cysteic acid builds from the outer cortex to the inner cortex, which further validates that bleaching is a diffusion-controlled process. FTIR-ATR studies with whole fiber hair tresses and 3-μm cross-sections showed that the cuticular cysteic acid concentration changes abruptly, whereas conversion of cortical cystine to cysteic acid is diffusion limited. Raman spectroscopy perfectly complemented FTIR-ATR and FTIR imaging, in which case Raman was used to directly follow changes in cystine (509 cm^{-1}) as a function of bleaching time, whereas FTIR spectroscopy monitored increases in cysteic acid concentration (1040 cm^{-1}). The cortical EDF values for Raman and FTIR spectroscopic techniques correlated linearly ($R^2 = 0.93–0.99$), whereas the association between whole tress and cortical EDF results was poor ($R^2 = 0.61–0.73$). For the series of bleached fibers, changes in the denaturation temperature (T_D) from HPDSC analyses obeyed Fick's laws of diffusion ($R^2 = 0.99$), where the diffusion constant was estimated to be 1.1×10^{-8} $cm^2 min^{-1}$. Using the peak in T_D, the model-free Ozawa method was applied to approximate changes in the activation energy of intermediate filament denaturation as a function of increasing bleaching time. After 90 min of bleaching, the HPDSC activation energies plateaued at 180 ± 8 kJ/mol against increasing cysteic acid concentration. Dry DSC results showed that conversion of cystine to cysteic acid increased the cortical mobility temperature, advocating that ionic and hydrogen-bonded networks stabilized components of the dry cortex during excessive heating. The MTGA pyrolysis onset temperatures ranged from 237°C to 248°C for virgin and 240 min bleached hair tresses,

Address all correspondence to Timothy Gillece, tgillece@yahoo.com

respectively, where the onsets positively and linearly correlated with increases in cysteic acid concentration ($R^2 = 0.95$); however, the activation energy for pyrolysis of dry fibers showed a curvilinear correlation with Raman EDF, with a peak activation energy (554 ± 9 kJ/mol) corresponding to 60–90 min bleaching times. To establish connections between water management properties and cystine oxidation, linear trends in denaturation temperature against the normalized Raman cystine band at 509 cm^{-1} demonstrated that decreased cross-link density is directly connected to greater steady-state moisture regains ($R^2 = 0.94$). For hair tresses, low EDF correlated with high tryptophan levels; however, with increased bleaching, tryptophan and cystine levels rapidly decreased. As expected, longer bleaching times produced increased differences in color, as indexed by ΔE.

INTRODUCTION

Hair bleaching is one of the most common chemical treatments of hair. This cosmetic procedure is carried out to lighten hair that is naturally dark. Therefore, the objective of such treatments is to destroy and remove melanin granules from the hair fiber. This is an oxidative process that is typically achieved with hydrogen peroxide (H_2O_2) and ammonia. Since melanin granules are in the cortex of hair, hair bleaching formulations must penetrate the fiber integument. Unfortunately, bleaching of hair results in collateral damage to lipids, proteins, and other structural components of the fiber. Regarding oxidative susceptibility, some of the most labile amino acids in keratin are methionine, tyrosine, threonine, and tryptophan. Even more susceptible to bleaching damage are cystine residues, which predominantly undergo oxidative fission of sulfur-sulfur (-S–S-) cross-links, resulting in the formation of salts of sulfur acids, including sulfenic acid (-SOH), sulfinic acid ($-SO_2H$), and sulfonic acid ($-SO_3H$). Most of the species are intermediates while sulfonic acid, which is frequently referred to as cysteic acid, is the predominate moiety remaining after normal bleaching cycles (1). The oxidation of disulfide bonds in hair has a significant influence on the various components of the fiber. In fact, the highest concentration of disulfide bonds in the hair fiber is in distinct lamellar layers of cuticle cells including the A-layer and exocuticle; however, in comparison to the cortex, the cuticle does not significantly contribute to the mechanical properties of hair since it is only a fraction of the total cross-sectional area. The cortex of hair is comprised of elongated cortical cells that are separated by a cell membrane complex. The cells are filled with macrofibrils containing low-sulfur intermediate filaments (crystalline phase) embedded in an amorphous matrix of cystine-rich proteins. Therefore, major targets of bleaching damage in the cortex are the disulfide bonds of the amorphous phase proteins.

Measurements including tensile strength, fatigue testing, vibrational spectroscopy, liquid retention, DSC, thermogravimetric analysis (TGA), scanning electron microscopy, and amino acid analysis, have been extensively used by researchers to survey chemical and structural damage to hair fibers as a function of alkaline bleaching treatments (2–19). In one of the earliest studies, Edman and Marti provided empirical evidence that hydrogen peroxide degrades disulfide bonds and diminishes the work required to stretch fibers (5). The investigators performed their tensile studies in distilled water to exclusively evaluate the influence of disulfide cross-links on the fiber modulus and to eliminate strength and resilience contributions from hydrogen and ionic bonding. Specifically, tensile testing provides modulus and breaking strength values for the hair fiber, where the overall hair fiber modulus involves contributions from hydrogen bonds, ionic bonds, and disulfide bonds (6). With this understanding, Robbins evaluated the wet tensile properties of bleached fibers from a single source and found that the wet tensile strength decreased by nearly 60% for

highly bleached fibers, where the compromised fibers were additionally found to have a 48% reduction in native cystine (1).

More recently, thermal analysis and vibrational spectroscopy have been used to further the thermochemical understanding of oxidative bleaching damage. Thermal analysis techniques, specifically DSC, differential thermal analysis, and TGA, have been extensively employed to probe melting and pyrolysis mechanisms in keratinous materials (6–14). In dry DSC experiments, snippets of dry hair fibers are heated to 250°–300°C and the intermediate filaments are consequently denatured and pyrolyzed in a coupled thermal event. Comparatively, in HPDSC experiments, water is added to the volume of hair fibers in hermetically sealed crucibles, wherein heating the cortex in excess water plasticizes the matrix and denatures the intermediate filaments at lower temperatures (e.g., 130°–155°C) than pyrolysis events (e.g., >210°C). Because the wet-matrix viscosity and associated cystine cross-links are directly related to denaturation temperatures measured in wet DSC, HPDSC provides a means to quantify the covalent cross-link density of the matrix (6,13). Vibrational spectroscopy has also been routinely used for studying oxidative hair damage and is typically less invasive and labor intensive than tensile testing protocols. Techniques including FTIR spectroscopy, FTIR imaging, and Raman spectroscopy have been applied to evaluate increases in cysteic acid, whereas confocal Raman spectroscopic imaging has been used to chemically image complementary decreases in disulfides bonds (16–18).

In the present work, results from FTIR chemical imaging, FTIR-ATR, and Raman spectroscopic measurements were compared with results from HPDSC, dry DSC, DVS, MTGA, colorimetry, and spectrofluorescence analyses to discern fundamental chemical structure/physical property relationships in chemically bleached hair fibers. Spectroscopic results were then leveraged to calculate the equivalent damage factor (EDF), which was applied to comparatively index bleaching damage in the cuticular and cortical compartments of the hair fiber.

MATERIALS AND METHODS

European dark brown and natural white hair tresses were bleached for 15, 30, 45, 60, 90, 120, and 240 min. Cysteic acid formation in peroxide-bleached whole fibers and cryotomed cross-sections was monitored using Raman and two FTIR spectroscopic techniques. In Raman analyses, the EDF was observed by following trends in the symmetric sulfonate (S = O) to phenylalanine ratio (1040/1003 cm^{-1}) and the attenuation in cystine (505–510 cm^{-1}) via the 509/1003 cm^{-1} band area ratio. Similar approaches were taken in FTIR-ATR spectroscopy and FTIR imaging, where the ratios of symmetric sulfonate (1040 cm^{-1}) to the cystine monoxide stretching band at 1080 cm^{-1} or amide II band (1548 cm^{-1}) were used to monitor cystine oxidation. In this work, both raw EDF and normalized EDF indices are reported. Raw EDF indices, which hereafter are referred to as EDF, were taken directly from protein-normalized cysteic acid spectral intensities, whereas normalized EDF results were evaluated to enable comparison of bleaching damage between spectroscopic techniques and band area/intensity normalizations. Normalized EDF calculations define EDF = 1.00 for nonbleached fibers, and accordingly the EDF indices for bleached fibers were always ≥1. These data were compared to results obtained from HPDSC, where endothermic transitions such as the denaturation temperature (T_D) and denaturation enthalpy (ΔH_D) were monitored. The T_D parameter correlates with changes in matrix viscosity and cross-link density, whereas ΔH_D

measures the energy required to break the interface between the matrix and intermediate filament keratin proteins (IFKPs) and the energy needed to denature IFKPs. Additionally, dry DSC, DVS, and MTGA were performed to further the understanding of bleaching kinetics and to provide correlations between keratin oxidation, cortical swellability, and cortical pyrolysis. Spectrofluorescence and colorimetry measurements were carried out on hair tresses to correlate changes in cuticular EDF with tryptophan degradation and ΔE.

MATERIALS

Studies were carried out on medium density European dark brown and natural white hair tresses that were purchased from International Hair Importers & Products Inc. (Glendale, NY, USA). The natural white fibers were used solely for the Raman scattering studies. The hair was supplied as large tresses constructed with rectangular pieces of wax, which secured the root ends of the hair fiber. From this large tress, ¾-in wide tresses were sampled as a function of bleaching time. Bleaching was carried out by mixing 120 g of Clairol Professional BW2 powder lightener (The Wella Corporation, Woodland Hills, CA, USA) with 147 mL of Salon Care Professional 20 Volume Clear developer (Arcadia Beauty Labs LLC, Reno, NV, USA). The resulting mixture was applied to damp hair. Bleaching was carried out for time periods of 15, 30, 45, 60, 90, 120, and 240 min. The 15, 30, 45, and 60 min bleaching experiments were accomplished using the same bleach mix and removing hair samples at selected intervals. The tresses bleached for 120, 180, and 240 min were placed in a freshly prepared bleach mix at 60, 120, and 180 min, respectively, and the 90 min sample was taken midway between the 60−120 min bleaching treatment. After each hour, the remaining tresses were thoroughly rinsed in warm tap water to remove water-soluble material prior to reimmersing the tress in fresh bleaching solution and restarting the bleaching clock. After the last bleaching step, each tress was thoroughly rinsed with 40°C tap water and then soaked in distilled water for 3 h to remove soluble leachate. The leachate removal step was repeated a total of five times for each tress. Finally, the tresses were air-dried overnight prior to subsequent analyses.

HAIR CROSS-SECTION PREPARATION

Quarter-inch wide excised samples of the tress were subjected to sectioning using a Leica CM3050 S (Leica Microsystems GmbH, Wetzlar, Germany) cryostat equipped with a high-profile sectioning head and Leica 818 high-profile cutting blades. Note that the cryostat blade was changed after each sample. For each sample, a 25-mm aluminum specimen disc was pre-equilibrated in dry ice (−78.5°C). A small section (1/8–1/4 in wide x 1−2 in length) of the ¾-in wide tress was removed from the center of the tress length. The tip end of the damp fiber section was then held straight and perpendicular against the platform of the disc. At the interface between the disc and tip end of the fiber bundle, a drop of distilled water was then added. The drop instantly crystallized, hence causing the tip end of the fiber bundle to adhere to the aluminum specimen disc. By pulling gently upward on the root end of the fibers and slowly adding water to the fiber bundle, a straight rod of ice-embedded hair was produced. Separately, each embedded sample was then mounted onto the specimen head (−30°C) of the cryostat, where the chamber temperature was equilibrated at −25°C.

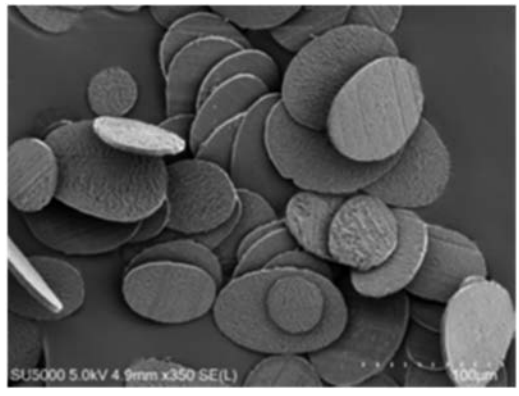

Figure 1. FESEM image of European dark brown hair fiber cross-sections (courtesy of W.T. Thompson, Ashland Specialty Ingredients, G.P.).

After conditioning for at least 1 h, 3- and 5-μm thick sections were collected in continuous mode using a sectioning speed of 60% maximum. Hair cross-sections were air-dried on paper overnight under reduced pressure. The cross-sections in Figure 1 demonstrate the intrinsic ellipticity of the European dark brown hair fibers.

FESEM OF HAIR FIBER CROSS-SECTIONS

The cross-sections were imaged using field emission scanning electron microscopy (FESEM) to determine the quality of the sections prior to FTIR imaging and to calculate the cortical cross-sectional area ($n = 100$). Cross-sections were fixed to aluminum PELCO® pin stubs (Ted Pella, Redding, CA, USA) using 25-mm conductive carbon tabs, and then coated with Au/Pd using our Leica EM ACE600 sputter coater. Finally, the staged fiber cross-sections were imaged with a Hitachi SU-5000 FESEM (Hitachi High Technologies, Schaumburg, IL, USA) using various magnifications. The virgin and bleached European dark brown hair cross-sections were elliptical (see Figure 1), with average major and minor diameters of 80 ± 10 μm and 57 ± 8 μm, respectively. Each fiber contained 5 ± 1 overlapping cuticle cells, and each cuticle cell was 380 ± 90 nm thick. The total pool of analyzed hair fiber cross-sections contained a mixture of medullated and non-medullated fibers.

STAGING OF HAIR FIBER CROSS-SECTIONS

Prior to FTIR imaging, hair fiber cross-sections must be properly staged on 25-mm calcium fluoride (CaF_2) windows (Spectral Systems LLC, Hopewell Junction, NY, USA). A Thermo Fisher Scientific (Waltham, MA, USA) stereo microscope and wooden toothpick were used to move cross-sections into place. In general, approximately 30 cross-sections were carefully juxtaposed without overlap on the CaF_2 crystal surface.

FTIR IMAGING OF 5-μm HAIR FIBER CROSS-SECTIONS

FTIR images were obtained with a Perkin-Elmer Spotlight 400 FTIR imaging microscope (Waltham, MA, USA), which combines an optical microscope with an FTIR spectrometer. The system consists of a linear array of mercury cadmium telluride detectors coupled to a precision automated X-Y sampling stage. Background spectra were collected on sample-free areas of the CaF_2 crystal, and FTIR images were obtained at 8 cm^{-1} spectral resolution in transmittance mode at 16 scans/pixel. Cross-sectioned hair (5-μm thickness) was used to ensure a linear transmission detector response for the entire IR spectral range. For each of the scans, the spatial resolution of each pixel was 6.25×6.25 μm, where each pixel provided a complete mid-IR spectrum. FTIR maps were afterwards generated with ISys software (Malvern Panalytical Ltd., Malvern, UK). The concatenated images were then baseline corrected from the base of the amide I band to 900 cm^{-1} prior to truncation of the spectra and images (150×150 μm). The resulting spectra were processed with GRAMS AI software (Thermo Fisher).

FTIR-ATR SPECTROSCOPY OF 3-μm HAIR FIBER CROSS-SECTIONS

A Perkin-Elmer Frontier FTIR spectrometer equipped with deuterated-triglycine sulfate detection, and a Perkin-Elmer universal attenuated total reflectance (ATR) accessory was used for all experiments. Small volumes of cryotome-generated 3-μm thick cross-sectioned hair fibers were compressed with a controllable pressure arm against the crystal face of the single-bounce ZnSe ATR crystal. Each spectrum was collected with 64 scans at 4 cm^{-1} resolution with one level of zero-filling. Perkin-Elmer Spectrum software automatically corrected for water and CO_2 atmospheric contributions, wherein no further vapor correction was needed for subsequent spectral analyses. The resulting spectra were processed with GRAMS AI software.

In separate measurements, to evaluate changes in the cuticle composition, complete hair tresses were pressed against the ATR crystal (i.e., cuticles against the crystal). In this case, the goal was to measure oxidative changes to the cuticle of the fiber. Each spectrum was obtained as described previously.

RAMAN SPECTROSCOPY OF 3-μm HAIR FIBER CROSS-SECTIONS

Raman spectroscopic measurements were performed with a Perkin-Elmer Raman Station 400 F equipped with 785 nm laser excitation. Natural white bleached hair samples that had been micronized to 3-μm sections, as described in the "Hair Cross-Section Preparation" section, were collected, blended, and consolidated for Raman scattering. Blended sections were poured into fresh aluminum DSC pans and loaded into the well plate module for sampling with the Raman laser, which was oriented in the vertical position. Typically, 10 accumulations of 60 sec were performed, with 90 sec exposures occasionally used when photo-bleaching of some background fluorescence was appropriate. As expected in Raman vibrational spectroscopy, the spectral range of the experiment was from 3500–100 cm^{-1}. Spectra were processed with GRAMS AI software.

HPDSC OF HAIR FIBER SNIPPETS

A TA Instruments (New Castle, DE, USA) Q2000 DSC and Perkin-Elmer high-volume pressure pans (3-part assembly, part numbers: top 0319-1526, bottom 0319-1525, and O-ring 0319-1535) were used for all HPDSC studies. The fibers were cut into 2–3 mm pieces with titanium precision shears. Approximately 10 ± 0.5 mg of fibers were loaded into high-volume steel crucibles and dried in our 60°C forced-air oven for 1 h. The fiber mass was reweighed and 50 μL of distilled water was added to the dried snippets using a micropipette. The pan was then loaded onto the center depression of the spacer insert and crimped with a Perkin-Elmer Quick Press. For each of the nine hair tresses, at least five pans were prepared ($n \geq 5$). Samples were equilibrated in the sealed pans for ≥12 h prior to being individually loaded into the indium-calibrated DSC cell using an automated sample cassette and robot. Several thermal ramping rates (β) were applied in this study. As per Istrate et al. (13), the T_D and ΔH_D of hair in excess water were evaluated using the following protocol:

1. Equilibrate at 20°C.
2. Isothermal for 2 min.
3. Ramp β °C/min to 180°C, where $\beta = 0.5$, 1.0, 2.0, 5.0, and 10°C/min were applied in the study.

The Flynn–Wall–Ozawa method with the peak in T_D was applied to approximate the activation energy for denaturation of the IFKPs. The ambient humidity was 28–32% relative humidity (RH).

DRY DSC OF HAIR SNIPPETS

A TA Instruments Q2000 DSC was used for the dry DSC work. The temperature and cell constant were calibrated using high-purity indium, and the heat capacity (C_p) was calibrated using sapphire discs. The control and bleached fibers were cut into 1–2 mm lengths and stabilized at 35% RH. Between 4 and 6 mg of fibers were loaded into aluminum Tzero pans (TA Instruments). No lids were used to permit the rapid release of pyrolysis gases. Two experiments were performed in the dry state. In the first, the fibers were equilibrated at 150°C for 5 min (to remove free water) before ramping to 325°C at 2°C/min. The data from the first experiment were used to monitor the peak in heat capacity as a function of temperature. In the second set of experiments, the fibers were equilibrated at 150°C for 5 min before ramping to 325°C at 15°C/min. The higher ramp rate produced the doublet endotherms, where the integrated area of the second endotherm was used to estimate the enthalpy for pyrolysis of the matrix (7).

MTGA OF HAIR SNIPPETS

A TA Instruments Discovery Series TGA with TRIOS control and analysis software (v3.3.1.4668) was used for all testing. The experiments were performed in modulated mode with high resolution ramp constraints. In dynamic high-resolution mode, the heating ramp rate is machine-adjusted such that the faster heating rate is used in temperature regions where no mass change is occurring, and a slower ramp rate is applied with the onset of mass changes. In MGTA, a sinusoidal temperature modulation is superimposed on the

heating ramp, and the sample-mass change in response to the modulation is recorded. The response provides an empirical tool for studying the kinetics of sample volatilization and/or decomposition. Discrete Fourier transform of the response allows kinetic parameters such as activation energy and pre-exponential factors to be calculated on a continuous basis. Unused snippets (4–6 mg) from the HPDSC experiments were loaded onto clean platinum TGA pans and the following protocol was used to denature and pyrolyze the samples: the furnace was equilibrated at 40°C; high-resolution sensitivity = 1.00; modulation temperature amplitude = 5°C; period = 200 s; high-resolution ramp = 5°C/min to 300°C; and resolution = 6.0. The hair fibers were denatured and pyrolyzed in a dry nitrogen environment (flow rate = 25 mL/min).

DVS OF 5-μm HAIR FIBER CROSS-SECTIONS

Water vapor absorption curves were obtained using a DVS Advantage I sorption analyzer (Surface Measurement Systems NA, Allentown, PA, USA) and microtomed cross-sections of virgin and bleached European dark brown hair (see "Hair Cross-Section Preparation" section). All experiments were conducted at 25°C with a nitrogen gas flow of 200 mL/min. The 5-μm thick microtomed cross-sections (4–6 mg) were loaded into a stainless steel mesh sample pan, and the following sorption-desorption procedure was applied:

1. Initial drying: 60°C and 0% RH for 1 h.
2. Isothermal equilibration: 25°C and 0% RH for 15 min.
3. Absorption curve: the microtomed fibers were subjected to increasing humidity in 10% RH steps from 0% to 90% RH with dm/dt = 0.002%/min for 15 min.
4. Desorption curve: after the absorption sequence, the water vapor was progressively desorbed from the sample by lowering the humidity in 10% RH steps from 90% to 0% RH with dm/dt = 0.002%/min for 15 min.

SPECTROFLUORESCENCE MEASUREMENTS OF HAIR TRESSES

Tryptophan levels in chemically treated hair were determined by carrying out fluorescence measurements using a Horiba Jobin Yvon (Edison, NJ, USA) FluoroMax-4 steady-state spectrofluorometer equipped with a bifurcated fiber optic probe. Spectra were collected directly from the surface of hair, approximately 1 in from the bottom of the wax portion of the hair tress (corresponding to the area of the tress proximal to the root). The emission and excitation slits were set at 5-nm bandpasses. The measurements were performed in emission mode, where tryptophan emission spectra were obtained by irradiating hair at 290 nm and monitoring the fluorescence emission at 339 nm. Data were provided in units of counts per second (cps), and the emission at 339 nm was normalized by taking the height ratio of tryptophan to kynurenine fluorescence (I_{339}/I_{440}), or the height ratio of kynurenine to tryptophan fluorescence (I_{440}/I_{339}). Average values were obtained by taking three measurements in neighboring zones of one hair tress.

SPECTROCOLORIMETRY OF HAIR TRESSES

To quantify the degree of color changes resulting from bleaching treatment in hair, we used a HunterLab ColorQuest XE spectrocolorimeter (Hunter Associates Laboratory, Inc.,

Reston, VA, USA). The use of the spectrocolorimeter enabled us to obtain the tristimulus (L, a, b) values, which were utilized to calculate discoloration parameters for describing color changes in the bleached hair. The data are reported in terms of the total color difference:

$$\Delta E = \sqrt{(\Delta L)^2 + (\Delta a)^2 + (\Delta b)^2} \quad (1)$$

Like the spectrofluorescence studies, three measurements obtained from one hair tress (approximately 1 in below the wax tab) represent the average reported values.

RESULTS AND DISCUSSION

In the current work, chemical bleaching was carried out on large (10 × 8 in) European dark brown hair tresses for a total of 4 h. At designated time intervals, including 15, 30, 45, 60, 90, 120, 180, and 240 min of continuous oxidative bleaching, samples were taken from the larger tress to assess the relationship between bleaching application times and changes to the chemical components of the hair fiber. For each sample, various spectroscopic and thermal analyses were conducted on whole fibers, short fiber snippets, and cryotomed fiber cross-sections.

As much of this study utilized vibrational spectroscopy for insights into the molecular and kinetic aspects of hair bleaching, Table I (16–19) provides some convenient and relevant mid-IR and Raman shift band assignments. We report an EDF parameter that indexes the degree of damage to cystine residues (-S—S-) in hair (19). The EDF parameter is based on the 1040 cm^{-1} symmetric -S=O sulfonate ($-SO_3^-$) stretching vibration band. However, as the intensity of individual FTIR-ATR spectra may vary, the 1040 cm^{-1} band intensity must be normalized to another invariable band in the mid-IR spectrum of the protein to ensure meaningful sample-to-sample comparisons. One approach is to ratio the 1040 cm^{-1} band to the 1080 cm^{-1} band (cystine monoxide stretch) in the mid-IR region. A potential difficulty in choosing the 1080 cm^{-1} band for normalization is that confounding

Table I
Mid-IR and Raman Band Assignments Pertinent to Hair Bleaching

Band assignment	Mid-IR (cm^{-1})(16,19)	Raman shift (cm^{-1})(16–18)
Amide I, α-helix	1650	1652 (16), 1671 (cuticle) and 1666 (cortex)
Sulfonate, S–O symmetrical stretch	1040, 1042 (19)	1040
Cystine monoxide (R–SO–S–R)	1075–1080	—
Sulfonate, S–O asymmetrical stretch	1175	—
Cystine dioxide (R–SO_2–S–R)	1229	—
Amide III (N–H stretch)	1247	1245 (cuticle) and 1243 (cortex)
CH_2 scissoring	1448–1454	1440 (16), 1451 and 1465 (cuticle) and 1448 (cortex) (18)
Amide II (C–N stretch, α-helix)	1547–1548	—
Amide I (C=O stretch, α-helix)	1650–1655	1652 (α-helix) (16), 1671 (cuticle) and 1659 (cortex)
N–H (primary amine)	3315	—
-S—S-	—	505 (cuticle) (17) and 507–509 (cortex)
-C—S-	—	664 (cuticle and cortex)
Phenylalanine of keratin	—	1004 (16), 1001–1003 (cuticle and cortex)

Figure 2. Photograph of (1) European dark brown hair, and European dark brown hair bleached for (2) 15 min, (3) 30 min, (4) 45 min, (5) 60 min, (6) 90 min, (7) 120 min, (8) 180 min, and (9) 240 min. For the series of tresses, a plot of ΔE as a function of the kynurenine fluorescence intensity (I_{440}/I_{339}) resulted in a linear relationship of increasing slope with very good correlation ($R^2 = 0.91$).

contributions from hair, including various sources of C—O stretching and phosphates from nuclear remnants, may interfere with accuracy; additionally, using the 1080 cm^{-1} absorption band may be inappropriate when formulated additives are included in the studies (20). For this reason, the ratio between 1040 cm^{-1} and the amide II band at 1548 cm^{-1} was used as an alternate method for normalizing the 1040 cm^{-1} spectral marker. Note that the applied measurement technique, specific analyses, and local conformations slightly shifted the peaks representing the protein vibrational bands.

FTIR IMAGING OF HAIR CROSS-SECTIONS

Samples from the bleached tresses, which are displayed in order of increasing bleaching time in Figure 2, were sectioned as described in the "Hair Cross-Section Preparation" experimental section and arranged on CaF_2 crystals for optimal staging in the FTIR microscope. FTIR spatial maps were then collected, and the series of images were concatenated to produce a single standardized chemical image. The color bar spectrum in Figure 3 represents the sulfonate concentration range in the concatenated image, where dark blue specifies the lowest concentration, and green, yellow, and red specify

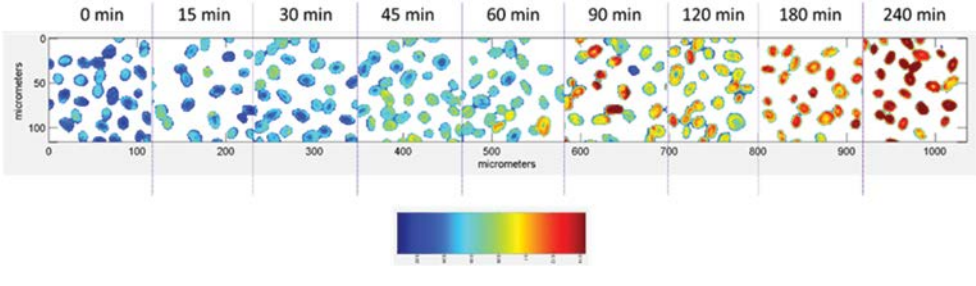

Figure 3. Concatenated images of hair fiber cross-sections treated for the indicated times with a bleaching formula. The color bar denotes the mid-IR 1040/1080 cm^{-1} normalized band area intensity, where the dark-red color specifies the highest level of cysteic acid in the 2D image of a cross-section.

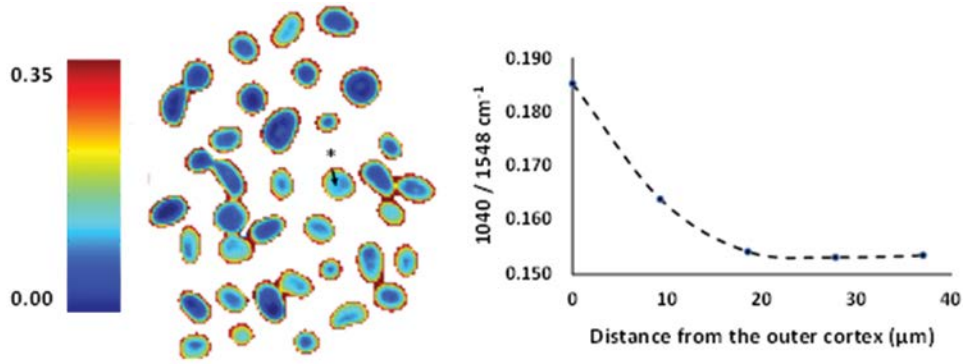

Figure 4. FTIR image and 1D EDF gradient for the 120 min bleached cross-sections. Relative to the concatenated FTIR image in Figure 3, which was normalized to 1080 cm^{-1}, the 1040 cm^{-1} cysteic acid band was instead normalized to the 1548 cm^{-1} amide II spectral marker. A representative gradient for a single cross-section (*) is shown. The EDF is highest at the outer cortex (0 μm) and lowest at the center of the cross-section (37 μm). The results specify that the cysteic acid concentration is highest near the cuticle and lowest near the center of the cross-section.

increasingly higher levels of cysteic acid. Hence, cysteic acid levels in the fibers increased with increasing bleaching time, and the intensity of the 1040/1080 cm^{-1} band area ratio increased accordingly.

Comparing the 120 and 180 min bleaching steps, the cysteic acid spatial concentration increased from the outer cortex to the inner cortex, which corroborates that bleaching is a diffusion-controlled process (1). Interestingly, the medulla was largely free of cysteic acid, where the deficiency in $-SO_3^-$ was likely a function of obstructed cortical diffusion, lower cystine concentrations, and lower medullar protein density, where keratin concentrations are comparably lower in the medulla (1,21). To exemplify the resultant cysteic acid gradient in the bleached cortex, Figure 4 demonstrates the spatial distribution of cysteic acid in the 120 min bleached cross-sections. Normalizing the 1040 cm^{-1} marker to the amide II band clearly emphasizes the compartmentalization of the fiber, where the boundaries of the cuticle, cortex, and medulla are readily observable. Additionally, the neighboring scatter plot in Figure 4 details the 1D spatial distribution of cysteic acid within the cortex of a single cross-section, which is identified by an asterisk. As judged by the color bar and 1040/1548 cm^{-1} scatter plot intensities, the cuticles clearly presented the highest intensities of oxidized cystine, while the centers of each cortex exhibited relatively lower levels of cysteic acid. Further, the scatter plot shows that the cysteic acid concentration was highest in the outer cortex (near the cuticle) and lowest near the center of each cross-section. Although only the 120 min bleached sample is detailed, note that all bleaching times conveyed similar 1D radial cysteic acid distributions.

Figure 5A contains a partial IR imaging spectrum (1900–900 cm^{-1}) for a virgin European dark brown tress (0 min bleached) obtained from an individual pixel from the cortex of its chemical image. The dashed vertical line is centered on the 1040 cm^{-1} absorption band, where the intensity changes proportionally with cysteic acid levels. Figure 5B shows the equivalent pixel spectrogram for the 240 min bleached sample in which the 1040 cm^{-1} band intensity has increased due to 240 min of chemical oxidation and resultant scission of keratinous disulfide.

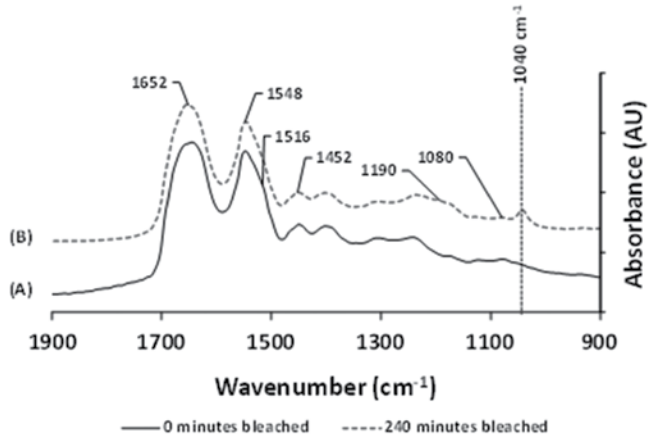

Figure 5. Example FTIR imaging spectra (1900–900 cm^{-1}) for the unbleached control (Tress 1 in Figure 1) and 240 min bleached European dark brown hair (Tress 9 in Figure 1). The dashed line is centered on the 1040 cm^{-1} band, which corresponds to changes in the cysteic acid concentration. AU: arbitrary units.

FTIR-ATR OF HAIR CROSS-SECTIONS

Figure 6 shows the 1040/1548 cm^{-1} band height ratios against bleaching time for data generated by loading layers of 3-μm thick cross-sections onto the 1.5 mm diameter ZnSe single-reflection ATR crystal. Both band height and area ratios were measured, yielding equivalent analysis results. For simplicity, the protein content was normalized without using the 1071–1080 cm^{-1} cystine monoxide band; instead, the EDF ratio was obtained from the 1040 cm^{-1} absorption intensity and the α-keratin component of the amide II band at 1548 cm^{-1} (see Table I). Substituting the amide II band for 1080 cm^{-1} ensured that the calculated EDF ratios were free of interference from neighboring IR absorptions, where the 1080 cm^{-1} band baseline is frequently infringed upon by (1) very strong -S=O absorptions emanating from the shoulder of the asymmetric sulfonate peak at approximately 1190 cm^{-1}; (2) unwanted contributions from nuclear remnants (PO_2^-); and (3) -C—O- functional groups belonging to extraneous sources. Lightly compressing the cylindrical

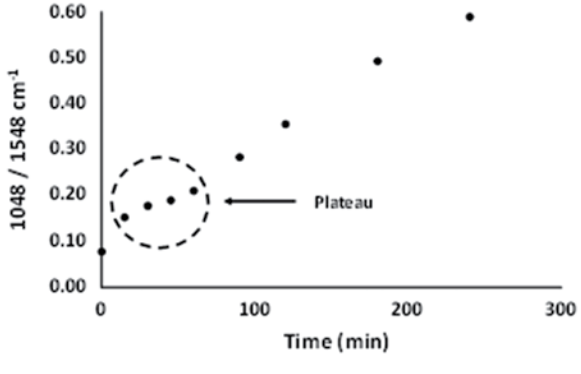

Figure 6. Plot of the 1040/1548 cm^{-1} EDF band ratio obtained from FTIR-ATR cortex studies. The 1548 cm^{-1} component of the amide II band was chosen to normalize protein content. The encircled plateau in first 60 min was likely due to ageing of the bleaching solution.

hair fiber cross-sections against the ATR crystal was used to take advantage of the 23:1 diameter-to-thickness aspect ratio, ensuring that the sections laid flat and the predominant signal originated from the cortex and medulla, with minimal contributions from the cuticle. Further, FESEM micrographs were used to estimate that the cross-sections were approximately 93.1 ± 1% ($\mu m^2/\mu m^2$) cortex, based on calculations using the average cross-sectional areas of the cortex and cuticle. Hence, the resultant spectra possessed excellent signal-to-noise ratios. Figure 6 summarizes the trends over the entire bleaching period. In the first treatment step (i.e., ≤60 min), there was an increase in cysteic acid, which was followed quickly by a short plateau after approximately 15 min of bleaching. The subsequent rate of damage (i.e., increasing cortical cysteic acid) then increased linearly through the remaining 180 min of treatment with the addition of fresh bleaching solution every 60 min.

FTIR-ATR AND SPECTROFLOURESCENCE OF HAIR TRESSES

To contrast FTIR-ATR analyses performed on collections of 3-μm cross-sections, the EDF ratio was also calculated from FTIR-ATR spectra measured with a single, whole hair tress. In this measurement, a portion of the uncut whole tress was pressed against the single-reflection ATR crystal. In an FTIR-ATR experiment with perfect contact, the evanescent wave from the IR source penetrates approximately 1–2 μm into the sample, meaning that only the cuticles are probed when performing FTIR-ATR on hair tresses; therefore, unlike the FTIR-ATR experiment on cross-sections, this measurement provided spectra that solely represent the chemistry of the hair cuticle (see spectra in Figure 7). Further, during the bleaching process, the alkaline bleaching solution was in persistent, intimate contact with the perimeter of the fibers. Hence, we anticipated the cuticle to rapidly oxidize in the initial bleaching steps. Figure 8 summarizes the whole hair tress FTIR-ATR results and displays trends in the EDF calculated from the 1040/1548 cm^{-1} band ratio, showing that the rate of cysteic acid formation over the 4 h bleaching period is indeed nonlinear. Note that correlations with the 1040/1080 cm^{-1} band ratio obtained from hair tresses presented identical results (see EDF in Figure 8).

Like hair tress ATR measurements, spectrofluorimetry of complete hair tresses is a means to study compositional changes to proteins on the fiber surface after applying cosmetic

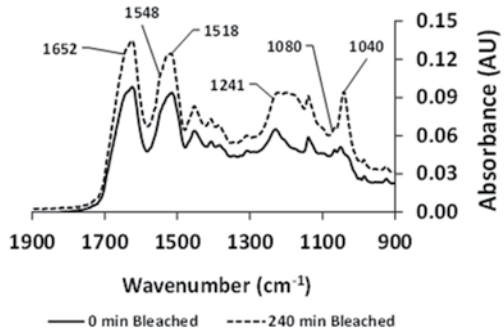

Figure 7. FTIR-ATR spectra for virgin (0 min bleached) and 240 min bleached whole-hair tresses. In previous work, the amide III (1241 cm^{-1}) and cysteine monoxide (1080 cm^{-1}) keratin bands had been used for cysteic acid (1040 cm^{-1}) band normalization (16–19).

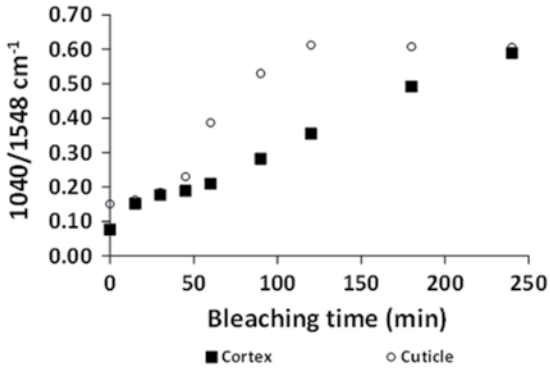

Figure 8. Overlay of the cortical 1040/1548 cm^{-1} band height ratio (EDF) obtained from FTIR-ATR cross-sectional and whole hair tress FTIR-ATR analyses. The whole fiber (cuticle) cysteine-sulfonic acid ratio changed abruptly, whereas the cortical cysteic acid concentration linearly increased as a function of applied bleaching time.

treatments. For example, tryptophan has been used as a fluorescence probe to monitor changes to keratin after chemical bleaching (22). In alkaline bleaching, the overall fluorescence of the fiber increases due to the degradation of melanin, which allows other chromophores in the hair to absorb light accompanied by fluorescence emission. Hence, to obtain meaningful data from fluorescence spectra, tryptophan peak intensities (I_{339}) were normalized to kynurenine (I_{440}). In our bleaching studies, the ratio of tryptophan to kynurenine fluorescence (I_{339}/I_{440}) decreased, indicating that surface tryptophan had been damaged and subsequently converted into kynurenines. In contrast, the ratio of kynurenine to tryptophan fluorescence (I_{440}/I_{339}) increased with increasing bleaching time. As was demonstrated with our FTIR-ATR whole fiber cystine oxidation studies, alkaline bleaching rapidly oxidizes labile surface amino acids, including keratinous tryptophan, where Figure

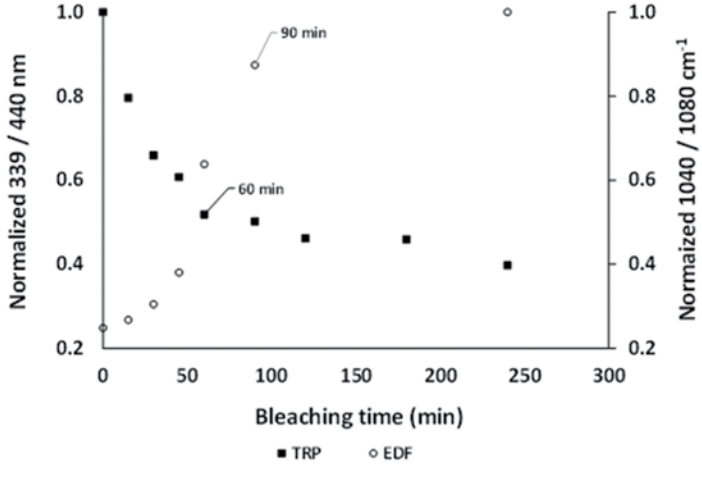

Figure 9. Hair tress normalized EDF (FTIR-ATR: 1040/1080 cm^{-1}) and normalized tryptophan/kynurenine fluorescence (I_{339}/I_{440}) versus bleaching time. TRP: tryptophan.

9 reveals a steep decrease in normalized tryptophan with proportional increases in whole fiber cysteic acid.

In contrast to whole fiber bleaching kinetics, oxidizing cystine in the cortical volume, which is encapsulated within the cuticle, was diffusion controlled, where the cuticular barrier initially mediated cortical absorption of alkaline peroxide. One possible explanation for the early plateauing of cortical FTIR-ATR data (first 60 min, Figure 8) is that the bleaching solution formed a viscous semisolid toward the end of each 1 h bleaching step, thereby hindering the rate of peroxide/persulfate cortical permeation. Consequently, the cuticle versus cortical EDF kinetical comparison for the FTIR-ATR studies (Figure 8 overlay), as judged by augmentation in the intensity of the normalized 1040 cm^{-1} cysteic acid band, is quite unambiguous. Initially, the cuticle received the brunt of the bleaching impact, whereas oxidative changes to the cortex were limited by tortuous permeation gateways introduced by cuticle and cortical diffusion networks. The disparity between the cuticle and cortical cysteic acid response is reconcilable when looking at each compartment of the hair fiber. While the morphology and molecular structure of the cuticle make it a formidable barrier for larger molecules, smaller molecules such as water, H_2O_2, and persulfates readily permeate the fiber structure, where diffusion control regulates further cortical permeation. Furthermore, excessive bleaching subsequently induces interfacial chemical attacks, leading to the formation of pores, cracks, and zones of erosion in the cuticle and cortex, thereby disturbing the natural diffusion processes and increasing the overall hydrophilicity of the fiber (23). As a result, trends in Figure 8 provide a "broad brush" for predicting subsequent physical properties that would be altered by cystine scission and the associated formation of cysteic acid.

RAMAN SPECTROSCOPY OF CROSS-SECTIONED HAIR

As the same cross-sectioning techniques for FTIR imaging and FTIR-ATR spectroscopic examinations were applied to the Raman studies, the high aspect ratio of the 3-μm thick cross-sections assured that the Raman spectra were predominantly composed of cortical and medullar shift frequencies. In the Raman experiments, instead of using European dark brown tresses, European natural white hair was employed because European dark brown hair contains melanin granules that induce excessive fluorescence, therein making it difficult to resolve Raman shifts for virgin or lightly-bleached dark brown fibers.

Prior work in confocal Raman spectroscopy and multivariate curve resolution analyses provides insights toward assigning the spatial assignment of functional groups to either the cuticle or cortex (17,18). These spectral markers allow for some specificity of band assignments in the work reported by this laboratory. A table of published Raman active band assignments is presented in Table I. Works by both Kuzuhara, as well as Pudney et al., infer exclusivity of certain vibrational modes as a function of their placement in either the cuticle or cortex (17,18). Examples of such domains in the Pudney work include bands in the 650 cm^{-1} (-C—S-, gauche) and 880 cm^{-1} spectral regions of the cuticle, and conversely, the 742 cm^{-1} CH_2 in-phase and 1002–1003 cm^{-1} phenylalanine bands that prominently appear in the cortex. Of course, many vibrational bands discussed in this study are shared between physical regions, such as the 1451 cm^{-1} C—H bending and 1650–1675 cm^{-1} amide I bands. While Kuzuhara's study agrees with Pudney on the specificity of some bands, including 1342 cm^{-1} (-CH_2 bend), he generally found the presence of most signature Raman bands, such as phenylalanine (1003 cm^{-1}), in both domains of

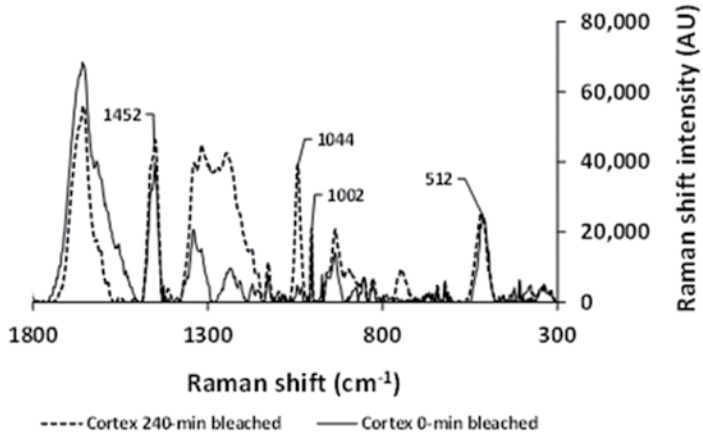

Figure 10. Raman shift intensity spectra for 0 and 240 min bleaching times. Note the appearance of the 1044 cm^{-1} ($-SO_3^-$) peak after bleaching the fibers for 240 min.

the Raman hair map. In fact, the Kuzuhara results align with amino acid analysis work published by Robbins, which advocates that phenylalanine is present in both the cuticle and cortex (1). Although the bulk Raman methodology used in our studies does not offer the compartmental selectivity asserted in the confocal studies of Pudney, the work is in line with Kuzuhara. For example, the 1003 cm^{-1} phenylalanine band was present in the cuticle as well as the cortex, which is assumed to be the bulk of the cross-sectioned fiber. With some exceptions, both cortex spectra from cross-sections (assuming cuticle contributions do not exceed 7–8% of the total signal) and cuticles largely reflect their spatial origination with superior signal-to-noise ratios over their confocal Raman microscopy counterparts.

With the reasoning stated previously, Figure 10 displays overlaid Raman spectra from microtomed hair cross-sections collected at 0 and 240 min bleaching times. Immediately visualized is the increase in the 1040 cm^{-1} band intensity at 240 min bleaching. It should be noted that some background fluorescence in the 0 min bleached sample made the loss in the 509 cm^{-1} shift band a little less apparent; however, integrating both band intensity

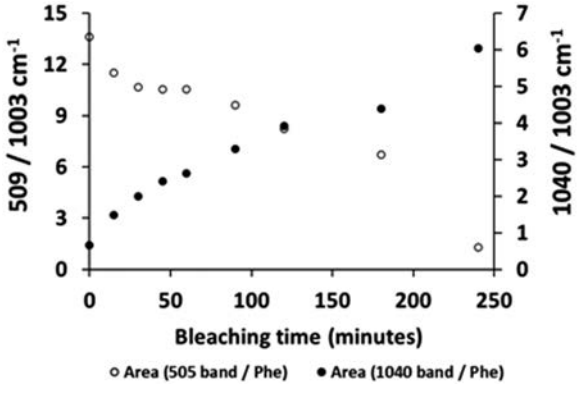

Figure 11. Raman scattering shifts as a function of bleaching time. Note the complimentary decrease in -S—S- (cystine) and increase in $-SO_3^-$ (cysteic acid). Phe: phenylalanine (1003 cm^{-1}).

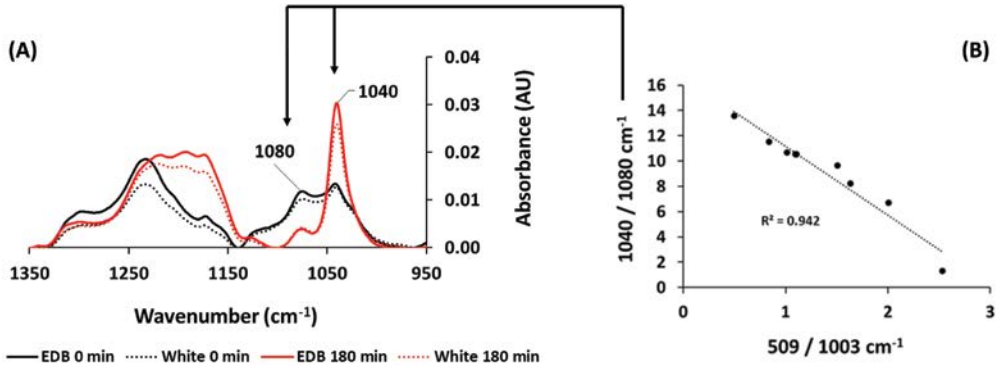

Figure 12. (A) Overlay of FTIR spectra for virgin European dark brown and natural white hair cross-sections bleached for 0 and 180 min. For each hair type, the spectra of virgin and bleached cross-sections are virtually identical; and (B) comparison of EDF and EDF^{-1} evaluations from FTIR imaging and Raman scattering, respectively. EDB: European dark brown; White: Natural white.

areas against the area of the phenylalanine band at 1003 cm^{-1} allowed for a quantitative probe of hair bleaching effects. Quantitatively, Figure 11 traces the content of the two essential indicators of the hair cortex structural integrity, namely the states of disulfide and cysteic acid plotted as a function of bleaching time. These indicators are visualized through the intensity (area) of vibrational bands for disulfide linkages (-S—S-) at 509–511 cm^{-1} and the cysteic acid band (-S—O- stretch) at approximately 1040 cm^{-1}. The plotted intensity response of these bands is elegantly complimentary, displaying the disulfide intensity loss due to cystine-bond scission, accompanied by the increase in intensity of the cysteic acid band at 1040 cm^{-1}, which together corroborate oxidative bleaching damage. To verify the integrity of the band normalization, the ratio of the 509 cm^{-1} and 1040 cm^{-1} bands to the 1450 cm^{-1} band were also calculated, yielding equivalent trends (17). The progression in intensity for the 509 cm^{-1} and 1040 cm^{-1} indicator bands conveys a distinct sigmoidal response to applied bleaching time. This change is particularly pronounced at shorter bleaching times, with an acceleration and apparent plateauing noted in the first hour. As mentioned in the infrared results, the nonlinear response segment between 15 and 60 min of bleaching may relate to the effects of bleach solution viscosity, sampling artifacts, or to the delayed swelling behavior of the fiber (i.e., due to increased alkalinity) in the early moments of the treatment. Agreement between Raman and FTIR bleaching kinetics is demonstrated by comparing the FTIR 1040 cm^{-1} cysteic acid band intensities, which are measurable with FTIR and Raman, to the 509 cm^{-1} -S—S- band intensity obtained exclusively from Raman scattering. Comparing the spectral markers in the virgin and 180-min bleached dark brown and natural white hair cross-sections, Figure 12A indicates that melanin granules and/or solubilized melanin remnants in dark brown hair negligibly influenced the height and area of the FTIR-ATR 1040 and 1080 cm^{-1} spectral EDF bands. In addition, Figure 12B compares the 1040/1080 cm^{-1} integrated band intensity ratio from FTIR imaging (using dark brown hair cross-sections) against the Raman 509/1003 cm^{-1} integrated shift ratio (using natural white hair cross-sections). The results for two completely different sets of experiments yielded a reasonably linear result ($R^2 = 0.94$), thus validating the ability to interweave EDF data from the Raman and FTIR techniques.

Summarizing, equivalent damage factors were calculated from cortical and cuticular cysteic acid versus keratin band area normalizations. To contrast spectroscopic techniques and

Table II
Normalized Cortical EDF Ratios Versus Bleaching Time as Indexed from Various Spectroscopic Methods

Bleaching time (min)	Raman cortex[a] 1040/1003 cm^{-1}	ATR cortex[a] 1040/1548 cm^{-1}	Imaging cortex[a] 1040/1548 cm^{-1}	Imaging cortex[b] 1040/1650 cm^{-1}	Imaging cortex[b] 1040/1080 cm^{-1}
0	1.00	1.00	1.00	1.00	1.00
15	2.25	1.34	1.36	1.10	1.68
30	3.04	1.49	1.44	1.14	2.04
45	3.66	1.61	1.69	1.21	2.20
60	4.00	1.83	1.97	1.26	2.23
90	5.03	2.44	2.42	1.32	3.04
120	5.99	3.29	3.72	1.39	3.29
180	6.68	4.27	4.44	1.43	4.04
240	9.19	5.34	5.21	1.50	5.09

[a]Normalized by band area.
[b]Normalized by band height.

band intensity evaluations, normalized EDF values for each bleaching time are displayed in Tables II and III, where normalized EDF values were calculated using Equation 2. Table II includes normalized cortical EDF values, and Table III contains normalized whole hair tress EDF indices.

$$Normalized\ EDF = \frac{Band\ normalized\ 1040\ cm^{-1}\ intensity\ for\ bleached\ fibers}{Band\ normalized\ 1040\ cm^{-1}\ intensityfor\ unbleached\ fibers} \quad (2)$$

where normalized EDF ≥ 1 for bleached hair, and band normalized 1040 cm^{-1} refers to indexing the 1040 cm^{-1} intensity to the 1003, 1080, 1548, and 1650 cm^{-1} protein bands, as described in the "Raman Spectroscopy of Cross-Sectioned Hair" and "FTIR-ATR of Hair Cross-Sections" sections. Overall, EDF values increased with increasing bleaching time. The cortical EDF values for Raman against FTIR techniques correlate linearly ($R^2 = 0.95–0.99$), independent of the band chosen for normalization. Similarly, if the 0 and 15 min bleaching

Table III
Normalized Whole Hair Tress EDF Ratios Versus Bleaching Time as Indexed from the Various Spectroscopic Methods

Bleaching time (min)	Raman whole fiber[a] 1040/1003 cm^{-1}	ATR whole fiber[a] 1040/1080 cm^{-1}	ATR whole fiber[a] 1040/1548 cm^{-1}	Raman whole fiber[a] 1040/1650 cm^{-1}	Spectrofluorimetry (TRP)[b] 440/339 nm intensity
0	1.00	1.00	1.00	1.00	1.00
15	1.65	1.23	1.08	1.71	1.26
30	4.49	1.53	1.23	4.19	1.52
45	4.97	2.25	1.53	5.93	1.65
60	6.84	2.89	2.57	8.46	1.93
90	7.93	3.70	3.52	9.79	1.99
120	8.31	4.00	4.06	10.55	2.17
180	8.19	4.35	4.03	10.89	2.18
240	8.34	4.40	4.02	11.74	2.52

[a]Normalized by band area.
[b]Normalized by band height.

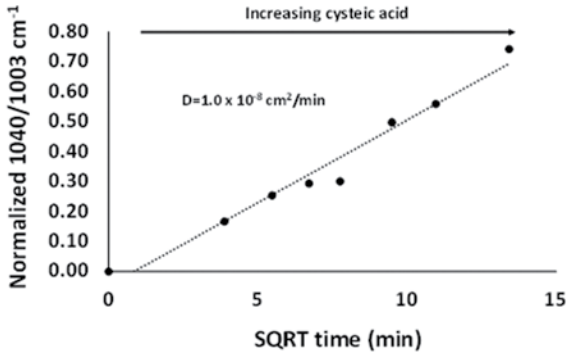

Figure 13. Diffusion plot for the normalized Raman EDF band height versus square root of bleaching time. SQRT: square root.

steps are removed (due to small Raman fluorescence artifacts), linear correlations between Raman and FTIR-ATR whole hair fiber EDF analyses are excellent, with $R^2 = 0.93–0.98$. More importantly, spectral correlations between whole tress and cross-sections analyses are weaker, when judged solely by the magnitudes of scatter plot correlation coefficients ($R^2 = 0.60$-0.78). In the "FTIR-ATR of Hair Cross-Sections" and "Raman Spectroscopy of Cross-Sectioned Hair" sections, we applied aspect-ratio arguments to justify the use of cross-sections spectra as solely describing chemical changes in the cortex. To complete the rationalization, note that spectra from FTIR chemical imaging of cross-sections were sampled solely from pixels of the hair fiber cortex. Hence, *stronger* correlations between FTIR imaging and FTIR-ATR/Raman cross-sections spectra, and *weaker* correlations between FTIR imaging and whole fiber analyses further support the acceptable use of "cortical" when describing the spectral analyses of hair fiber cross-sections. Finally, we have been synonymously referring to the normalized 509 cm^{-1} band as EDF; more accurately, however, the Raman 509/1003 cm^{-1} band ratio is roughly EDF^{-1}, where *increases* in cysteic acid are proportional to *decreases* in cystine (e.g., Figures 11 and 12).

Figure 13 looks at the process of cystine bleaching damage through Fick's laws of diffusion, where a substance is said to follow Fickian diffusion if the normalized solute uptake linearly relates with the square root of process time (24). Figure 13 contains a plot of the process-normalized Raman cysteic acid scattering intensity (1040/1003 cm^{-1}) against the square root of bleaching time. The approximate diffusion coefficient (D) for bleach consumption, as monitored by the conversion of cystine to cysteic acid, was evaluated as 1.1×10^{-8} $cm^2 min^{-1}$. The approximate diffusion coefficient was evaluated from the slope of the graph and the average cross-sectional fiber radius (1,24). The linearity of cortical oxidation with the square root of time generally agrees with the visual interpretation displayed by the FTIR micro-spectroscopic spatial maps exhibited in Figure 3.

HPDSC ANALYSIS OF BLEACHED HAIR

In the HPDSC method for analyzing the state of hair keratin, snippets of hair are soaked in water and then heated through the denaturation temperature in sealed stainless steel crucibles. By thermally insulting the fiber cortex in the wet state rather than the dry state, water plasticization of the cortical matrix separates denaturation and pyrolysis events (6–15). T_D probes the plasticity and viscosity of the matrix, whereas ΔH_D represents the

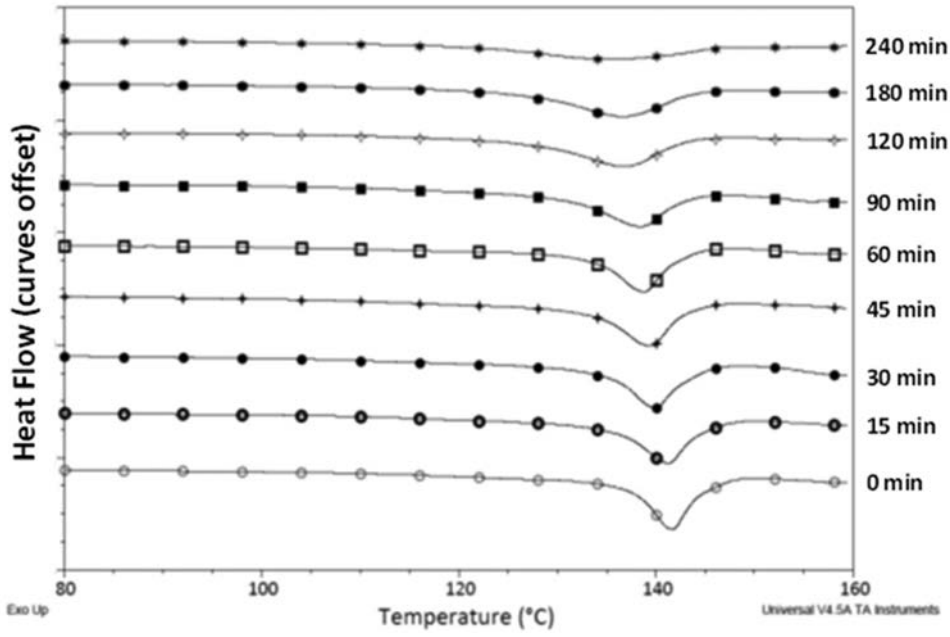

Figure 14. Effect of bleaching on the denaturation temperature and the shape of the enthalpy peak. The curves have been vertically offset for visual clarity ($\beta = 2$°C/min).

energy required to denature the *interphase* and α-helical keratin, where Popescu and Istrate describe the interphase as the covalent linkage between the IFKPs and the intermediate filament associated proteins (IFAPs) (8,13).

Figure 14 provides $\beta = 2$°C/min HPDSC thermograms for hair subjected to increasing bleach exposure time. The endotherm between 120°C and 150°C is characteristic for wet hair fibers and when integrated provides a measurement of ΔH_D. The position of the endotherm along the temperature axis yields T_D. Note the shift in T_D to lower temperatures as the bleaching time is increased. Further, the width of the endotherm peak broadens,

Table IV
Summary of HPDSC Data for the Bleached Samples ($\beta = 2$°C/min)

Bleaching time (min)	T_D (°C)	ΔH_D (J/g)
0	141.3 ± 0.6	19.8 ± 0.5
15	139.7 ± 0.3	19.8 ± 0.3
30	139.5 ± 0.3	19.7 ± 0.5
45	139.2 ± 0.5	19.8 ± 0.8
60	139.4 ± 0.3	19.5 ± 0.4
90	138.3 ± 0.3	18.9 ± 0.4
120	137.1 ± 0.3	17.6 ± 0.3
180	136.3 ± 0.4	15.8 ± 0.7
240	134.6 ± 0.7	10.7 ± 0.8

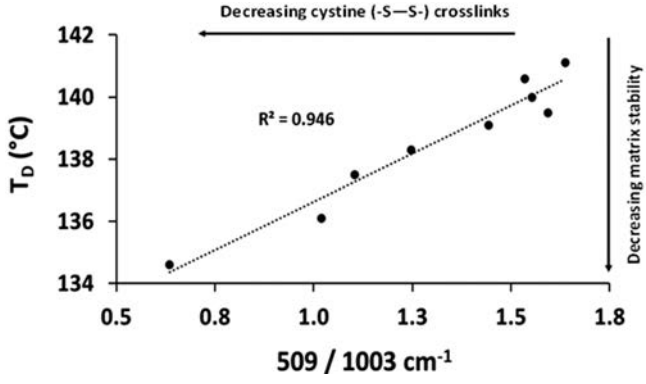

Figure 15. Correlation of wet DSC denaturation temperature with Raman EDF^{-1} (band height ratio).

suggesting that the intrinsic chemical environment of the amorphous and crystalline keratins had been degraded to a continuum of residual conformational states. For example, in the control sample, the onset of degradation started at temperatures above 135°C; however, in the 240 min bleached sample, denaturation began at approximately 120°C.

Table IV summarizes the HPDSC analyses performed on the 2–3 mm snippets of bleached hair exhibited in Figures 2 and 14. As surmised by gradual changes in T_D and little change in ΔH_D, the data in Table IV demonstrate that bleaching initially influenced the highly cross-linked amorphous IFAPs and disulfide-based IFKP–IFAP linkages rather than denaturing the crystalline structure of the IFKPs. However, dramatic changes in the crystalline and amorphous contents were noted at longer bleaching times (≥120 min). Hence, the progression of cystine to cysteic acid was steady, yet the crystalline IFKPs in hair remained resilient until approximately the 2 h bleaching mark. The wet DSC T_D parameter correlates well with EDF results from FTIR imaging, FTIR-ATR, and EDF/EDF^{-1} from Raman spectroscopy cross-sectional work, where a decrease in T_D is proportional ($R^2 = 0.95$) to an increase or decrease in EDF or EDF^{-1}, respectively (see Figures 12 and 15). Hence, as reported in the literature, T_D directly relates to decreases in matrix cross-link density (7,8,13).

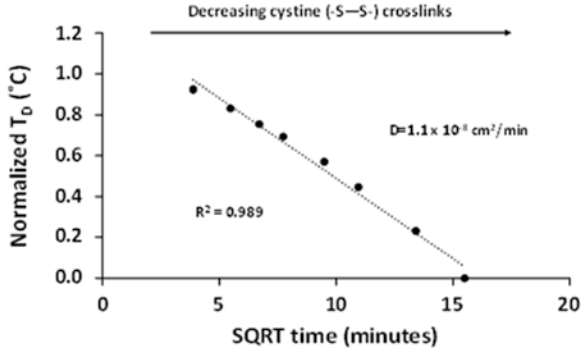

Figure 16. Correlation of normalized denaturation temperature with the square root of bleaching time.

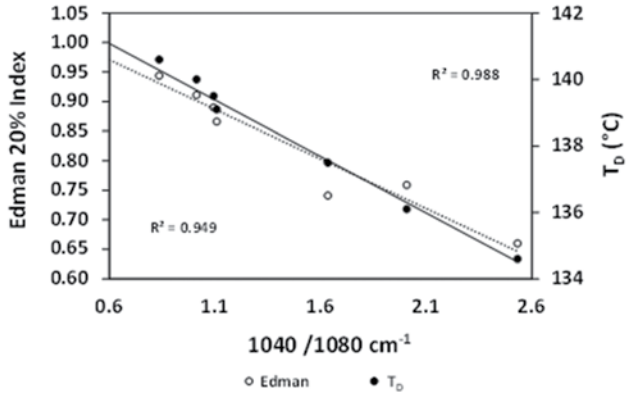

Figure 17. Correlation of Edman 20% Index ($R^2 = 0.95$) and T_D ($R^2 = 0.99$) data (from this work) with the FTIR imaging 1040/1080 cm^{-1} EDF results. Edman's 20% Index and T_D decrease proportionally with increasing bleaching time. Note that the magnitudes of bleaching time and cysteic acid increase with increasing 1040/1080 cm^{-1} ratio.

Regarding published associations between cystine degradation and mechanical testing, Robbins adapted data from Edman and Marti (5) to demonstrate that up to 45% of intrinsic cystine bonds are cleaved by aggressive hydrogen peroxide bleaching protocols. He concluded that decreases in the mechanical properties of peroxide-treated fibers were diffusion-controlled processes, where the calculated diffusion coefficient from tensile properties was assessed at 1.8×10^{-9} cm^2min^{-1}. Hence, since decreasing EDF^{-1} and T_D are proportional to losses in matrix cross-linking, and EDF^{-1} changes proportionally with T_D (Figure 15), by the transitive property of equality we expected T_D to obey Fick's law (1,24). Indeed, Figure 16 provides evidence of this correlation ($R^2 = 0.99$), where the diffusion constant was estimated at 1.1×10^{-8} cm^2min^{-1}, which closely agrees with D determined from Raman scattering results (Figure 13) and magnitudes of D presented in the literature (1,3,24,25,26). Furthermore, Edman and Marti were among the first researchers to theorize that the hair fiber cortex, and more specifically, the conversion of disulfide bonds to cysteic acid in the cortex are responsible for the loss in wet tensile properties as a function of bleaching time (1,5). They used the 20% Index test to report oxidative damage results. In the 20% Index test, the ratio of work required to stretch the fiber 20% after treatment is compared to the work required to stretch the fiber 20% before treatment. By chance, we used similar bleaching conditions and treatment times as Edman, where only the 90 min data point is not included in Edman's findings. Figure 17 contains the Edman 20% Index data and T_D plotted as a function of the 1040/1080 cm^{-1} FTIR imaging band ratio. The data indicate that decreased tensile work correlates with increasing bleaching time ($R^2 = 0.95$) and associated decreases in cortical cysteic acid. Further, with increased bleaching times, trends in T_D (wet fibers) positively correlate with wet tensile work results, where diminished cystine is the common element. Raman scattering experiments yielded similar results, but with a positive slope, where Figure 12B demonstrates the complementary FTIR versus Raman correlation.

By varying heating rates in HPDSC and assessing T_D, the activation energy for denaturation of bleached fibers may be assessed. ASTM E698 describes the Flynn–Wall–Ozawa model-free method for evaluating the activation energy by measuring temperatures corresponding to fixed conversion values (α) from experiments performed at different DSC heating rates. By plotting $ln(\alpha)$ against $1/T$, the slope gives $-E_a/R$, where R is the molar gas constant, and

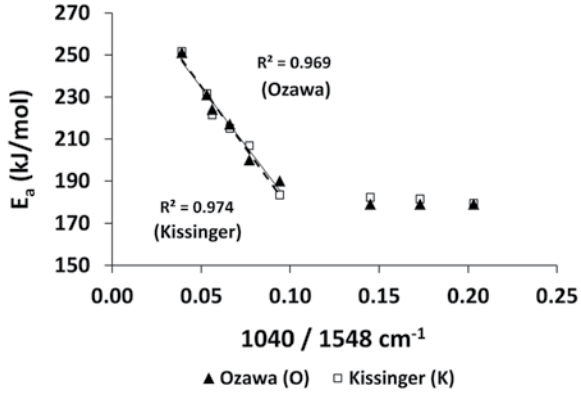

Figure 18. HPDSC Ozawa denaturation activation energy versus FTIR imaging EDF band area ratio. The E_a plateau at 180 kJ/mol is associated with bleaching times ≥120 min. The standard deviation is ± 13 kJ/mol. Results from the Kissinger method (using T_D) are overlaid with results from the OFW E_a analysis (27). The thermal measurements were performed in distilled water.

E_a is the activation energy for denaturation of α-keratin. By assuming that the denaturation mechanism is invariable at different heating rates, the peak in T_D may be used to approximate $\alpha = 0.5$ (8,27,28). Figure 18 demonstrates the correlation of the assessed E_a against the EDF determined by FTIR imaging. The results indicate that the energy barrier for denaturation decayed linearly for the first hour of bleaching ($R^2 = 0.99$) — after which, the activation energy plateaued at approximately 180 kJ/mol. The range of determined E_a values agrees with the literature; however, perhaps due to inherently complex multistep keratin denaturation processes, or to the source of our virgin European dark brown tresses, we observed a decrease in E_a, rather than an increase, with increased bleaching times (13,14).

DRY DSC OF BLEACHED HAIR FIBER SNIPPETS

In dry DSC experiments, no water is added to the DSC pans and denaturation and pyrolysis events are difficult to distinguish. Hence, we accepted that denaturation and pyrolysis were not

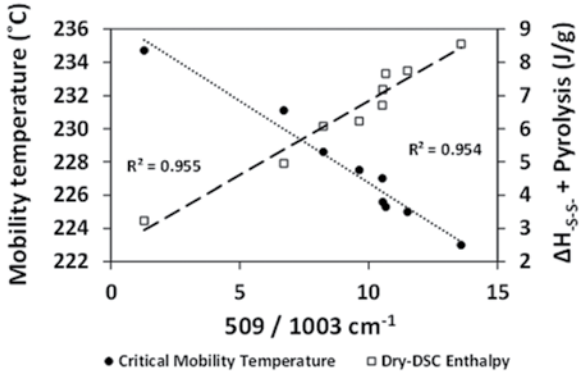

Figure 19. Dry DSC critical matrix mobility and denaturation/pyrolysis enthalpy versus Raman EDF^{-1}. The critical mobility temperature was assessed by the peak in C_p as a function of increasing temperature.

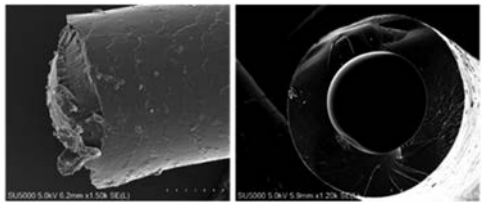

Figure 20. View of the cortex of a bleached fiber at temperatures >250°C. In the left image, note the cortical remnants that extruded from the interior of the fiber. In the right image, observe the reduction in cortical material and the persistence of the cuticle. At higher temperatures, the cortex was torn asunder and only the cuticle remained.

unique events and instead decided to use our sapphire-calibrated DSC to monitor continuous changes in C_p as a function of increasing temperature. Heat capacity changes are related to changes in mobility, where increases in sample mobility at lower temperatures are connected to decreased physical and covalent matrix cross-link density. Figure 19 shows that conversion of -S—S- to -SO_3^- appears to have *increased* the temperature of the apparent C_p inflection, meaning that ionic and hydrogen-bonded networks stabilized the dry-fiber cortex during applied heating. The peak in C_p linearly correlates with increasing cysteic acid ($R^2 = 0.96$), where the C_p maxima ranged from 223°C for the unbleached control to 234°C for the 240 min bleached sample. Figure 19 additionally graphs the dry DSC pyrolysis enthalpy against trends in the normalized Raman 509 cm^{-1} band and clearly demonstrates that more thermal energy is required to vaporize matrix components with higher levels of cystine ($R^2 = 0.95$). Hence, the formation of two moles cysteic acid from the scission of one mole of disulfide influences the disruption mechanism for cortical denaturation and pyrolysis. One plausible explanation is that after bleaching strongly acidic cysteic acid salts (pKa < 2) rearrange and form strong ionic cross-links with basic ammonium moieties in keratin. Consequently, modified denaturation/pyrolysis pathways are required to initiate cortical flow and pyrolysis of matrix protein (3,14). Figure 20 pictorially demonstrates the deleterious effects of excessive heating, which involved flow (left image) and the synchronous vaporization of cortical components (right image). To produce flow, scission of disulfide bonds in the matrix and interphase reduced the cross-link density and lowered the matrix viscosity to critical values. TGA-FTIR analysis of the gaseous pyrolysis effluent confirmed that flow was then activated by liberation of carbon dioxide gas (CO_2) from the degrading IFKPs, which pushed the molten components out of the durable microtubule. Along with other unpublished supporting micrographs, the right image suggests that vaporization occurred from the medulla outward, which is a result that had been previously reported in the literature (29).

MTGA OF BLEACHED HAIR FIBER SNIPPETS

MTGA combines nonlinear heating with a sinusoidal temperature program to obtain pyrolysis events and kinetic parameters in a single experiment. Furthermore, by combining modulation with dynamic high-resolution thermogravimetry, overlapping weight loss events may be more easily resolved. MTGA is a dry fibers testing technique, where hair fiber snippets are pyrolyzed at high temperatures in a 0% RH nitrogen environment. Figure 21 plots the activation energy for pyrolysis against cysteic acid concentration, where the bleaching times increase from left to right on the abscissa. Next to the E_a data are the MTGA pyrolysis onset temperatures, where the extrapolated onsets correlate positively and

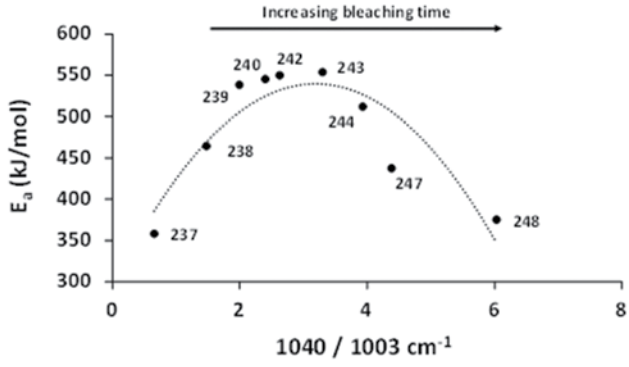

Figure 21. Activation energy (± 8 kJ/mol) from MTGA studies as a function of Raman EDF. The values next to the E_a data are the MTGA pyrolysis extrapolated onset values, which are in units of ± 0.5°C.

linearly with increases in cysteic acid ($R^2 = 0.95$). More specifically, the onsets to thermal denaturation/pyrolysis increased with increasing bleaching damage, where the 240 min bleached sample exhibited pyrolysis at 248°C, which was 11°C higher than demonstrated by the nonbleached fibers. Interestingly, E_a magnitudes show a curvilinear correlation with Raman EDF, with a peak E_a corresponding to 60–90 min bleaching. Hence, the energy barrier required to denature the IFKPs and pyrolyze the cortex was increased with minor increases in cortical ionic character. However, after 90 min of chemical bleaching, the E_a barrier began decreasing. Finally, at 240 min of bleaching, where cystine bonds are lessened by 40−50%, the barrier to pyrolysis was nearly equivalent to that of unbleached hair (1). Comparing the E_a and onset temperatures by MTGA to the Ozawa activation energy values and T_D determined by HPDSC, the trends are generally disparate, where the E_a values and temperatures to break ionic cross-links were lower when the fibers were heated under increasing pressure in excess water. For the virgin European dark brown fibers, the MTGA derived activation energy values for dry fibers (358 ± 6 kJ/mol) agree with published E_a results (416 ± 8 kJ/mol) determined using the non-reversing signal in modulated DSC; further, our E_a results (251 ± 7 kJ/mol) from HPDSC also followed Wortmann's results (263 ± 16 kJ/mol), where the E_a for the untreated dry fibers was 43% higher than the results obtained in wet HPDSC studies (14).

DVS OF BLEACHED FIBERS

Modifying the cross-link density, hydrophilicity, and porosity of the hair fibers induces subtle changes to the water management properties of hair. For example, chemical bleaching cleaves structural lipids from the F-layer of the cuticle and oxidizes cystine cross-links throughout the fiber. Consequently, bleaching increases whole fiber cysteic acid salt concentrations with commensurate increases in whole fiber wettability. In dry environments, secondary structuring between complementary side chains in oxidized keratin is strong; however, at higher humidity, water vapor solvates hydrogen bonds and ionic cross-links and accordingly influences the temporal dynamics of water vapor sorption. To establish connections between water-regain properties and cystine oxidation, Figures 15 and 22 together associate decreases in cross-link density (i.e., lower T_D) with greater steady-state moisture regains ($R^2 = 0.94$). For convenience, Figure 22 includes the inversely proportional DVS ($R^2 = 0.94$) and HPDSC ($R^2 = 0.92$) results against the Raman 509/1003 cm^{-1} band

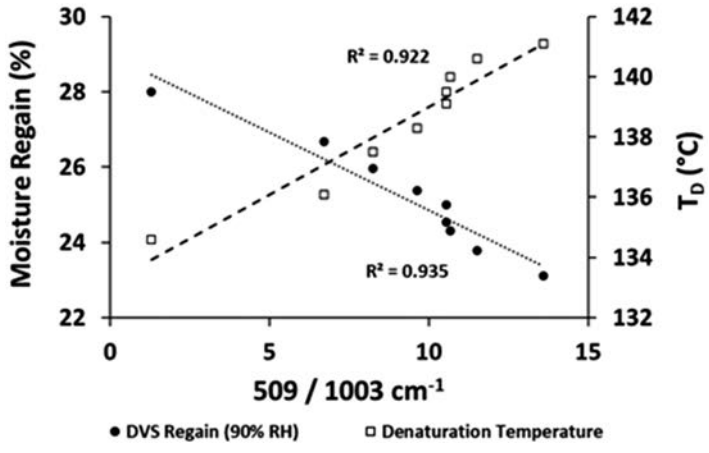

Figure 22. DVS maximum moisture regain (90% RH) and T_D against normalized disulfide content (normalized Raman 509 cm^{-1} band area intensity).

area intensity. Noting that dm/dt control with hair fibers produces kinetical and not fully equilibrated outcomes, Figure 22 details the maximum regains for the bleached samples at 90% RH, where the maximum adsorption difference between virgin and the 240 min bleached sample was approximately 6% (w/w) (30).

CONCLUDING REMARKS

Several instrumental techniques were applied to monitor physicochemical changes in hair fibers resulting from repetitive bleaching treatments. FTIR imaging provided a 2D map of the cysteic acid composition across the volume of individual fiber cross-sections. By operating in transmission mode, FTIR imaging demonstrated a visual footprint of chemical damage caused by oxidative bleaching, including compositional and conformational modifications to the cuticular, cortical, and medullar components of the fiber, while leveraging all aspects of the mid-IR spectrum for the entire thickness of each discrete cross-section. FTIR-ATR and Raman spectroscopy were used to probe collections of hair cross-sections and whole fibers for average cysteic acid and cystine changes. Marrying the spectroscopic techniques presented a means to correlate spectra from individual pixels in the cortex of single cross-sections with average spectra from multiple cross-sections obtained from FTIR-ATR and Raman spectroscopy studies. Further, by simply glancing at the concatenated FTIR image, color changes in adjacent panels were used to qualitatively describe the spatial progress of timed chemical bleaching, whereas EDF indices from FTIR-ATR and Raman spectroscopy facilitated quantitative associations between global chemical changes and thermomechanical outcomes, including correlations with Fickian diffusion. Most striking, as shown in Figure 8, is the stark difference between cuticle and cortex EDF kinetics that have been elucidated with these experiments. Additionally, colorimetry and fluorescence spectroscopy were used to quantify hair tress color changes and to correlate oxidative tryptophan degradation with increased bleaching time. Thermal measurements, including HPDSC, dry DSC, TGA, and DVS provided supportive physical characterization of the bleaching process and allowed us to better resolve the effects of chemical bleaching on the amorphous and crystalline

phases of the hair. When conditioned in dry ambient environments, cysteic acid moieties in keratin appear to bond ionically with proteinaceous residues, where the resultant physical cross-links within the fiber matrix are quite strong. Hence, many moderate-humidity thermomechanical measurements may not straightforwardly distinguish the effects of oxidative physiochemical fiber damage. However, in the wet state, water solvates hydrogen and ionic physical cross-links within the cortex and the residual thermomechanical strength is bestowed to the durability of the remaining disulfide bonds. Consequently, results from wet thermal and wet mechanical testing protocols accurately describe oxidative chemical damage; however, in the dry state, the effects of cystine oxidation may not directly correlate with results from routine mechanical testing.

ACKNOWLEDGMENTS

The authors would like to acknowledge Dr. Guojin Zhang for the virtual ISys lessons; T-bone Schiess, William Thompson, and Fan Wu of Ashland LLC; and Geddy Lee of Rush. Special thanks to Dr. Crisan Popescu for any results that we *properly* interpreted.

REFERENCES

(1) C. R. Robbins, *Chemical and Physical Behavior of Human Hair*, 4th Ed. (Springer-Verlag, New York, 2002), pp. 360–435.
(2) E. P. Everaert, S. Zhang, D. Tran, B. Kroon, G. Zhang, W. T. Thompson, and R. L. McMullen, 2015. Strengthening the hair fiber from within: repairing the cortex of damaged hair, Zurich, Switzerland, 21–23 Sept 2015. *23rd IFSCC Conference* accessed April 1, 2021, http://tst.pg2.at/abstracts/data/full_papers/full_paper_90.pdf.
(3) L. J. Wolfram, K. Hall, and I. Hui, The mechanism of hair bleaching, *J. Soc. Cosmet. Chem.*, **21**, 875–900 (1970).
(4) A. J. Grosvenor, S. Deb-Choudhury, P. G. Middlewood, A. Thomas, E. Lee, J. A. Vernon, J. L. Woods, C. Taylor, F. I. Bell, and S. Clerens, The physical and chemical disruption of human hair after bleaching—studies by transmission electron microscopy and redox proteomics, *Int. J. Cosmet. Sci.*, **40**, 536–548 (2018).
(5) W. W. Edman and M. E. Marti, Properties of peroxide-bleached hair, *J. Cosmet. Sci.*, **12**, 133–145 (1961).
(6) C. Popescu (June 16, 2016), The internal structure of hair and its interpretation by tensile strength and DSC measurements, *The Cosmetic Chemist*, accessed March 13, 2021, http://www.thecosmeticchemist.com/education/hair_care_technology/the_internal_structure_of_hair.html.
(7) C. Popescu and C. Gummer, DSC of human hair: a tool for claim support or incorrect data analysis, *Int. J. Cosmet. Sci.*, **38**, 433–439 (2016).
(8) D. Istrate, C. Popescu, and M. Möller, Non-isothermal kinetics of hard alpha-keratin thermal denaturation, *Macromol. Biosci.*, **9**, 805–812 (2009).
(9) F.-J. Wortmann, C. Popescu, and G. Sendelbach, Non-isothermal denaturation kinetics of human hair and the effects of oxidation, *Biopolymers*, **83**, 630–635 (2006).
(10) F.-J. Wortmann, G. Sendelbach, and C. Popescu, Fundamental DSC investigations of alpha-keratinous materials as basis for the interpretation of specific effects of chemical, cosmetic treatments on human hair, *J. Cosmet. Sci.*, **58**, 311–317 (2007).
(11) F.-J. Wortmann, C. Springob, and G. Sendelbach, Investigations of cosmetically treated human hair by differential scanning calorimetry in water, *J. Cosmet. Sci.*, **53**, 219–228 (2002).
(12) F.-J. Wortmann and H. Deutz, Characterizing keratins using high-pressure differential scanning calorimetry (HPDSC), *J. Appl. Polym. Sci.*, **48**, 137–150 (1993).
(13) D. Istrate, "Heat induced denaturation of fibrous hard alpha-keratins and their reaction with various chemical reagents." PhD thesis, RWTH Aachen. 2011.
(14) F.-J. Wortmann, G. Wortmann, J. Marsh, and K. Meinert, Thermal denaturation and structural changes of alpha-helical proteins in keratins, *J. Struct. Biol.*, **177**, 553–560 (2012).
(15) F.-J. Wortmann, A. Hullman, and C. Popescu, Water management of human hair, *Int. J. Cosmet. Sci.*, **30**, 388–389 (2008).

(16) G. Zhang, R. L. McMullen, R. Mendelsohn, and O. Musa, "Applications of Vibrational Spectroscopic Imaging in Personal Care Studies," in *Computational Optical Biomedical Spectroscopy and Imaging*, S. M. Musa. Ed. (CRC Press, New York, 2015), pp. 1–26.
(17) A. Kuzuhara, Analysis of structural change in keratin fibers resulting from chemical treatments using Raman spectroscopy, *Biopolymers*, **77**, 335–344 (2005).
(18) P. D. Pudney, E. Y. Bonnist, K. J. Mutch, R. Nicholls, H. Rieley, and S. Stanfield, Confocal Raman spectroscopy of whole hairs, *Applied Spectroscopy*, **67**, 1408–1416 (2013).
(19) V. Signori and D. M. Lewis, FTIR investigation of the damage produced on human hair by weathering and bleaching processes: implementation of different sampling techniques and data processing, *Int. J. Cosmet. Sci.*, **19**, 1–13 (1997).
(20) A. Barth, Infrared spectroscopy of proteins, *Biochim. Biophys. Acta.*, 1767, 1073–1101 (2007).
(21) R. McMullen, D. Laura, S. Chen, D. Koelmel, G. Zhang, and T. Gillece, Determination of physicochemical properties of delipidized hair, *J. Cosmet. Sci.*, **64**, 355–370 (2013).
(22) R. L. McMullen, S. Chen, and D. J. Moore, Spectrofluorescent characterization of changes in hair chemistry induced by environmental stresses, *J. Cosmet. Sci.*, **62**, 191–202 (2011).
(23) R. L. McMullen and G. Zhang, Investigation of the internal structure of human hair with atomic force microscopy, *J. Cosmet. Sci.*, **71**, 117–131 (2020).
(24) C. Barba, M. Martí, J. Carilla, A. M. Manich, and L. Coderch, Moisture sorption/desorption of protein fibres, *Thermochim. Acta*, **552**, 70–76 (2013).
(25) C. Robbins and C. J. Kelly, Amino acid analysis of cosmetically altered hair, *J. Cosmet. Sci.*, **20**, 555–564 (1969).
(26) M .L. Tate, Y. K. Kamath, S. B. Ruetsch, and H.-D. Weigmann, Quantification and prevention of hair damage, *J. Cosmet. Sci.*, **44**, 347–371 (1993).
(27) C. Popescu and E. Segal, Critical considerations on the methods for evaluating kinetic parameters from nonisothermal experiments, *Int. J. Chem. Kinet.*, **30**, 313–327 (1998).
(28) T. Ozawa, Kinetic analysis of derivative curves in thermal analysis, *J. Therm. Anal. Calorim.*, **2**, 301–324 (1970).
(29) D. Istrate, M. E. Rafik, C. Popescu, D. E. Demco, L. Tsarkova, and F.-J. Wortmann, Keratin made micro-tubes: the paradoxical thermal behavior of cortex and cuticle, *Int. J. Biol. Macromol.*, **89**, 592–598 (2016).
(30) T. A. Evans, "Adsorption Properties of Hair," in *Practical Modern Hair Science*, T. A. Evans and R. R. Wickett. Eds. (Allured Books, Carol Stream, IL, 2012), pp. 333–365.